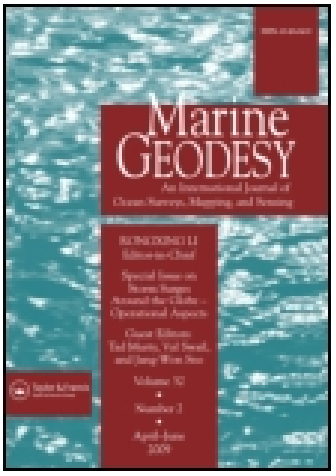

Marine Geodesy
Publication details, including instructions for authors and subscription information:
http://www.tandfonline.com/loi/umgd20

Estimating ENSO Influence on the Global Mean Sea Level, 1993-2010

A. Cazenave [a], O. Henry [a], S. Munier [a], T. Delcroix [a], A. L. Gordon [c], B. Meyssignac [a], W. Llovel [b], H. Palanisamy [a] & M. Becker [d]
[a] LEGOS, OMP, Toulouse, France
[b] JPL, Pasadena, California, USA
[c] LDEO, Columbia University, New York, New York, USA
[d] UMR Espace-DEV/UAG, Cayenne, French Guiana
Published online: 18 Dec 2012.

To cite this article: A. Cazenave, O. Henry, S. Munier, T. Delcroix, A. L. Gordon, B. Meyssignac, W. Llovel, H. Palanisamy & M. Becker (2012) Estimating ENSO Influence on the Global Mean Sea Level, 1993-2010, Marine Geodesy, 35:sup1, 82-97, DOI: 10.1080/01490419.2012.718209

To link to this article: http://dx.doi.org/10.1080/01490419.2012.718209

Marine Geodesy, 35(S1):82–97, 2012

ISSN: 0149-0419 print / 1521-060X online
DOI: 10.1080/01490419.2012.718209

Taylor & Francis
Taylor & Francis Group

Estimating ENSO Influence on the Global Mean Sea Level, 1993–2010

A. CAZENAVE,[1] O. HENRY,[1] S. MUNIER,[1] T. DELCROIX,[1]
A. L. GORDON,[3] B. MEYSSIGNAC,[1] W. LLOVEL,[2]
H. PALANISAMY,[1] AND M. BECKER[4]

[1]LEGOS, OMP, Toulouse, France
[2]JPL, Pasadena, California, USA
[3]LDEO, Columbia University, New York, New York, USA
[4]UMR Espace-DEV/UAG, Cayenne, French Guiana

Interannual global mean sea level (GMSL) variations and El Nino-Southern Oscillation (ENSO) are highly correlated, with positive/negative GMSL anomalies during El Nino/La Nina events. In a previous study, we showed that interannual GMSL and total land water storage variations are inversely correlated, with lower-than-average total water storage on land and higher-than-average GMSL during El Nino. This result is in agreement with the observed rainfall deficit/excess over land/oceans during El Nino (and vice versa during La Nina). It suggests that the positive GMSL anomaly observed during El Nino is likely due to an ocean mass rather than thermal expansion increase. Here, we analyze the respective contribution of the Atlantic, Indian, and Pacific oceans to the interannual (ENSO-related) GMSL anomalies observed during the altimetry era (i.e., since 1993) with an emphasis on the 1997/1998 El Nino event. For each oceanic region, we compute the steric contribution, and remove it from the altimetry-based mean sea level to estimate the ocean mass component. We find that mass changes of the tropical Pacific Ocean, mainly in the region within 0–25°N, are mostly responsible for the observed 1997/1998 ENSO-related GMSL anomaly. The ocean mass excess of this region almost perfectly compensates the total land water deficit during the 1997/1998 El Nino. An estimate of the ocean-atmosphere water balance of this region shows that the time derivative of the ocean mass component is well correlated with net P-E (precipitation minus evaporation) over most of the study period, except during the 1997/1998 ENSO event, where there is a temporary ocean mass increase, not compensated by the net P-E. We thus propose that the 1997/1998 ocean mass increase of this north tropical Pacific area be linked to an imbalance between the inflow/outflow entering/leaving the north tropical Pacific. A preliminary qualitative analysis indicates that a significant reduction of the Makassar Strait transport, (about 80% of the total Indonesian throughflow), as previously reported in the literature during the strong 1997/1998 El Nino event, could explain the north tropical Pacific Ocean mass excess reported in this study, hence the observed positive GMSL anomaly.

Keywords Sea level, ENSO, land waters, steric sea level, ocean mass

Received 13 January 2012; accepted 27 April 2012.
Address correspondence to Anny Cazenave, LEGOS, 18 Avenue Edouard Belin, 31401 Toulouse Cedex 9, France. E-mail: anny.cazenave@legos.obs-mip.fr

1. Introduction

On interannual to multidecadal time scales, global mean sea level (GMSL) variations can be explained by ocean thermal expansion and water mass variations (due to land ice melt and land water storage changes) (e.g., Bindoff et al. 2007). Over the altimetry era (1993–2010), the rate of GMSL rise amounts to 3.2 +/− 0.4 mm/yr (e.g., Ablain et al. 2009; Nerem et al. 2010) and is rather well explained by ocean thermal expansion (by ∼30%) and land ice loss (∼60%) (e.g., Cazenave and Llovel 2010; Church et al. 2011). So far, however, little attention has been given to explain the origin of the GMSL interannual variability. For the altimetry era, Nerem et al. (2010) noticed that detrended GMSL changes are correlated to El Nino-Southern Oscillation (ENSO) occurrences, with positive/negative sea level anomalies observed during El Nino/La Nina. This is illustrated in Figure 1a showing detrended altimetry-based GMSL over 1993–2010 and the Multivariate ENSO Index (MEI; Wolter and Timlin 1998). The correlation between the two monthly data sets is rather modest (equal to 0.4) for the whole time span but reaches 0.7 when the calculation is performed over the 1997–98 period including the very strong record-breaking 1997/1998 El Nino event. This suggests that ENSO influences either ocean thermal expansion or ocean mass (or both). Interestingly, Llovel et al. (2011a) reported that the interannual GMSL variations are inversely correlated to interannual variations in global land water storage, with a tendency for a deficit in land water storage during El Nino events (and vice versa during La Nina). This was shown through a global water mass conservation approach using Gravity Recovery and Climate Experiment (GRACE) space gravimetry data and the Interactions between Soil, Biosphere and Atmosphere–Total Runoff Integrating Pathways (ISBA-TRIP) global hydrological model developed at MeteoFrance (Alkama et al. 2010) to estimate land water storage changes over the altimetry era.

Continental waters are continuously exchanged between atmosphere, land and oceans through vertical and horizontal mass fluxes (precipitation, evaporation, transpiration of the vegetation, surface runoff, and underground flow). Conservation of total water mass in the climate system at interannual time scale (neglecting to a first approximation, the atmospheric reservoir as in Llovel et al. 2011a) leads to:

$$\Delta M_{ocean} \approx -\Delta M_{LW} \tag{1}$$

where ΔM_{ocean} and ΔM_{LW} represent changes with time of ocean mass and total land water storage due to total fresh water input/output from precipitation, evaporation-transpiration, and runoff. Total land water storage change can be further expressed in terms of equivalent sea level change by simply dividing the total continental water volume change by the mean surface of the oceans and changing its sign (i.e., multiplying by -1 to reflect that less water on land corresponds to more water in the oceans, and inversely). Figure 1b shows the total land water storage change over 1993–2008 (an update of Llovel et al. 2011a; see Section 2.3), expressed in equivalent sea level, superimposed to the detrended GMSL. We can note the good quantitative agreement between the two curves, in particular during the 1997/1998 El Nino event. This result is not surprising as it is known that during an El Nino, there is more rain over the oceans and less rain on land as reported by several studies (e.g., Dai and Wigley 2000; Gu et al. 2007; Gu and Adler 2011). The fact that the positive 1997/1998 GMSL anomaly is quantitatively explained by the negative total land water storage anomaly suggests that there is almost perfect water mass compensation between ocean and land during that period and that other processes (e.g., ocean heat storage change) are negligible.

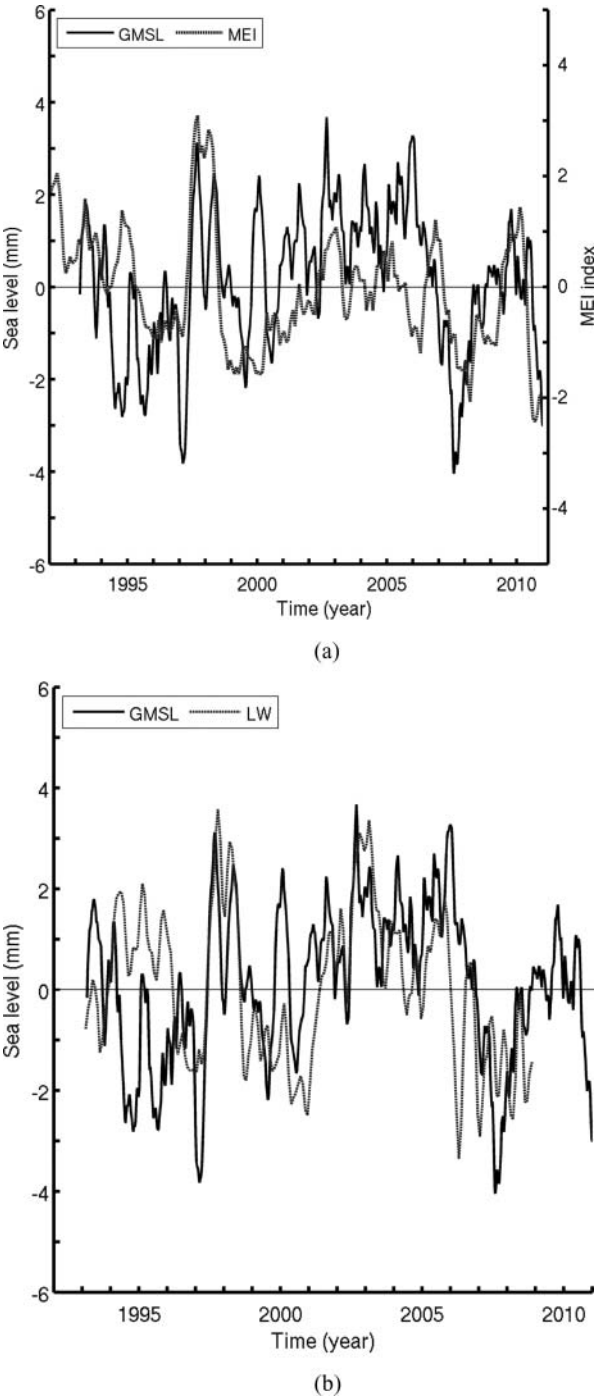

Figure 1. (a) Detrended altimetry-based global mean sea level (GMSL, black curve) and multivariate ENSO Index (MEI, black dotted curve). Positive MEI values denote El Nino periods, and negative values La Nina periods (b) Detrended altimetry-based global mean sea level (GMSL, black curve) and reversed (i.e., multiplied by -1) total land water storage from the ISBA-TRIP model expressed in equivalent sea level (LW, black dotted curve).

In the present study, we investigate this issue further and intend to determine whether the total ocean water mass excess noticed during El Nino is uniformly distributed over the oceans. If not, we want to know which ocean basin and/or region are mainly responsible for the ENSO-related GMSL anomalies. For that purpose, we consider the altimetry time span (since 1993) but mostly focus the discussion on the 1997/1998 ENSO event. We compute the detrended mean sea level in different oceanic regions, estimate the steric component (thermal expansion plus salinity effects) using in situ ocean temperature and salinity data, and deduce the ocean mass component for each region (from the difference between altimetry-based mean sea level and steric sea level). We find that it is the north tropical Pacific region that mostly contributes to the observed (anti) correlation between interannual GMSL and global land water storage during ENSO. We further estimate the water budget of the ocean-atmosphere system over the north Pacific region, considering the time derivative of ocean mass, precipitation P, evaporation E, and transport of water in and out the considered region. Finally we discuss potential processes causing the north tropical Pacific mass anomaly during ENSO.

2. Datasets

2.1. Sea Level Data

For the altimetry-based sea level data, we use the DT-MSLA "Ref" series provided by Collecte Localisation Satellite (CLS; http://www.aviso.oceanobs.com/en/data/products/sea-surface-height-products/global/msla/index.html). This dataset is used over the timespan from January 1993 to December 2010. It is available as 1/4° × 1/4° Mercator projection grids at weekly interval from a combination of several altimetry missions (Topex/Poseidon, Jason-1 and 2, Envisat, and ERS 1 and 2). Improved geophysical corrections are applied to the sea level data (see Ablain et al. 2009 for details).

2.2. Steric Data

Steric sea level is estimated using an updated version (v6.12) of in situ ocean temperature and salinity data from Ishii and Kimoto (2009) (called hereafter IK09). The IK09 temperature data are corrected for the XBT depth bias. The temperature and salinity data are available at monthly interval over 16 depth levels ranging from the ocean surface down to 700 m depth, on a global 1° × 1° grid from 1955 to 2009. Steric sea level anomalies are computed over the 0–700 m depth range for the period January 1993 to December 2009. The deep ocean contribution cannot be accounted for since hydrographic data below 700 m are too sparse, noting that recent studies showed that almost all interannual variability in steric sea level in confined in the upper 300–500 m of the ocean (e.g., Llovel et al. 2011b). At global scale, salinity does not contribute to the GMSL, but this is not true at regional scale. This is why here we account for salinity in this study.

2.3. ISBA-TRIP Global Hydrological Model

To estimate global land water storage, we use the ISBA-TRIP global hydrological model developed at MeteoFrance. The ISBA land surface scheme calculates time variations of surface energy and water budgets. Soil hydrology is represented by three layers: a thin surface layer (1 cm) included in the rooting layer and a third layer to distinguish between the

rooting depth and the total soil depth. The soil water content varies with surface infiltration, soil evaporation, plant transpiration, and deep drainage. ISBA uses a comprehensive parameterization of subgrid hydrology to account for heterogeneity of precipitation, topography, and vegetation within each grid cell. It is coupled with the Total Runoff Integrating Pathways (TRIP) module (Oki and Sud 1998). TRIP is a simple river routing model converting daily runoff simulated by ISBA into river discharge on a global river channel network here defined at 1° by 1° resolution. Details on the ISBA-TRIP model can be found in Decharme et al. (2006) and Alkama et al. (2010). The outputs of the ISBA-TRIP model cover the period January 1950 to December 2008, with values given at monthly interval on a 1°x1° grid. They are based on a forced mode run, with global meteorological forcing provided by the Princeton University on a 3-hourly time step and 1° resolution. We updated by two additional years (up to December 2008) the total land water storage computation done by Llovel et al. (2011a) using the ISBA-TRIP model. The whole land surface has been considered. The reversed total (i.e., whole land area-averaged) land water storage curve shown in Figure 1b (estimated from ISBA-TRIP model and expressed in sea level equivalent) has not been detrended (unlike the GMSL curve) because the land water storage trend is negligible. The correlation between the two curves is 0.4 over the whole period. It increases to 0.70 when considering the 1997–98 timespan (El Nino event).

2.4. Precipitation, Evaporation and Wind Stress Data

Precipitation P and evaporation E data used in this study are based on different datasets. For precipitation, we used products from the Global Precipitation Climatology Project (GPCP; Adler et al. 2003) and Climate Prediction Center Merged Analysis of Precipitation (CMAP; Xie and Arkin 1997). For evaporation, we used the Objectively Analyzed air-sea Fluxes product (OAFlux; Yu and Weller 2007) and the Hamburg Ocean Atmosphere Parameters and Fluxes from Satellite Data (HOAPS; Anderson et al. 2007). We also used reanalysis products from the European Centre for Medium-Range Forecast (ECMWF) ERA-Interim data (Simmons et al. 2007), which provides both precipitation and evaporation data. To give more confidence in the inferred net precipitation (P-E), we also estimated (P-E) using other parameters of the atmospheric moisture budget, namely precipitable water P_{water} and moisture flux divergence divQ (as done in several global- and regional-scale studies; e.g., Syed et al. 2009; Sahoo et al. in press). This was performed through the relationship:

$$P - E = -(dP_{water}/dt + divQ) \quad (2)$$

The P_{water} and divQ data were provided by the ECMWF ERA-Interim and the National Centers for Environmental Prediction/National Center for Atmospheric Research (NCEP/NCAR; Kalnay et al. 1996) databases.

These datasets provide monthly global data on regular grids (resolution from 0.5° to 2.5° depending on the dataset) in units of mm/month. All gridded data are further expressed in terms of monthly averages over the period January 1993 to December 2009.

2.5. Filtering, Averaging, Weighting, Smoothing and Data Uncertainties

As we focus here on the interannual variability, for all datasets we remove the seasonal signal at each mesh of all gridded fields (i.e., before area-averaging) through a least-squares adjustment of 6-month and 12-month period sinusoids. Mean time series are obtained by geographical averaging applying a cosine (latitude) weighting. To each spatially averaged

time series, we also remove a linear trend over the 1993–2009 timespan. A 3-month running filter is further applied.

Estimate of data uncertainties depends on the dataset. For altimetry-based sea level data, uncertainty of 3-month area-averaged sea level data is estimated to ∼1 mm (assuming a 4 mm error for 10-day mean values; see Ablain et al. 2009). The steric sea level error is estimated from the difference between the IK09 and Levitus et al. (2009) steric datasets. We find a mean error of ∼1.5 mm for the 3-month globally area-averaged steric sea level data. A similar approach is conducted to infer the P-E error using the differences between direct P and E estimates as well as indirect estimates from the atmospheric water balance equation (see Section 4.1).

3. Results: Contributions of Steric Sea Level and Mass Component to the Mean Sea Level in the Atlantic, Indian and Pacific Oceans, 1993–2010

We computed the spatially averaged, altimetry-based, and steric sea level, as well as mass component (i.e., the difference between altimetry-based mean sea level and steric component, assuming that the deep ocean contribution is negligible) over the: (1) Atlantic Ocean (70°W to 20°E; 60°S to 60°N latitude), (2) Indian Ocean (20°E to 120°E, 60°S to 30°N), and (3) Pacific Ocean (120°E to north and south America coasts, 60°S to 60°N). Figures 2a–c show the relative contributions of the Atlantic, Indian, and Pacific oceans to the interannual GMSL, as well as corresponding steric and ocean mass components. The term "relative contributions" means that each curve is weighted by the ratio between the surface of the considered area and the whole ocean surface (hereafter called "area weighting").

The contributions of the Atlantic, Indian, and Pacific sea level to the GMSL display significant interannual variability, with mean standard deviations of 1.1, 1.4, and 1.2 mm, respectively. Atlantic and Indian oceans show positive sea level anomalies peaking in 1998/early 1999, likely related to the La Nina phase that followed the 1997/1998 El Nino. These sea level anomalies are likely of thermal origin as the steric component closely follows the observed sea level. The correlation between mean sea level and steric sea level over 1997–98 is 0.75 and 0.67 for the Atlantic and Indian oceans, respectively, reinforcing the fact that during this El Nino period the sea level anomaly in these two basins has mostly a steric origin.

In late 1997/early 1998, the Pacific steric sea level is negative while the observed sea level is slightly positive. The correlation between the mean sea level and steric sea level is only 0.2 over 1997–98, contrasting with the higher correlation values discussed above for the Atlantic and Indian oceans.

The Pacific mass component presents a large negative anomaly in 1997 followed by a steep rise and a positive anomaly in early 1998. This result suggests that the 1997/1998 GMSL anomaly could be located in the Pacific Ocean.

To further infer the exact location of this mass anomaly, we computed the zonally averaged (from 120°E to the American coasts) time-latitude diagram of the Pacific Ocean mass anomalies (considering 1° wide latitudinal bands). The diagram is shown in Figure 3. It displays a positive anomaly in the ∼10°S–20°N latitude band during the 1994/1995 El Nino, followed by another positive anomaly during the 1997/1998 El Nino, located in the 5°S–30°N latitude band, and with an amplitude of ∼20 mm. The mass anomalies of this tropical band are then weaker or even slightly negative during the remaining time period that includes both El Nino and La Nina events.

From the diagram presented in Figure 3, we may conclude that the main 1997/1998 ENSO-related Pacific Ocean mass anomaly seen in Figure 2c is located in the 5°S–30°N

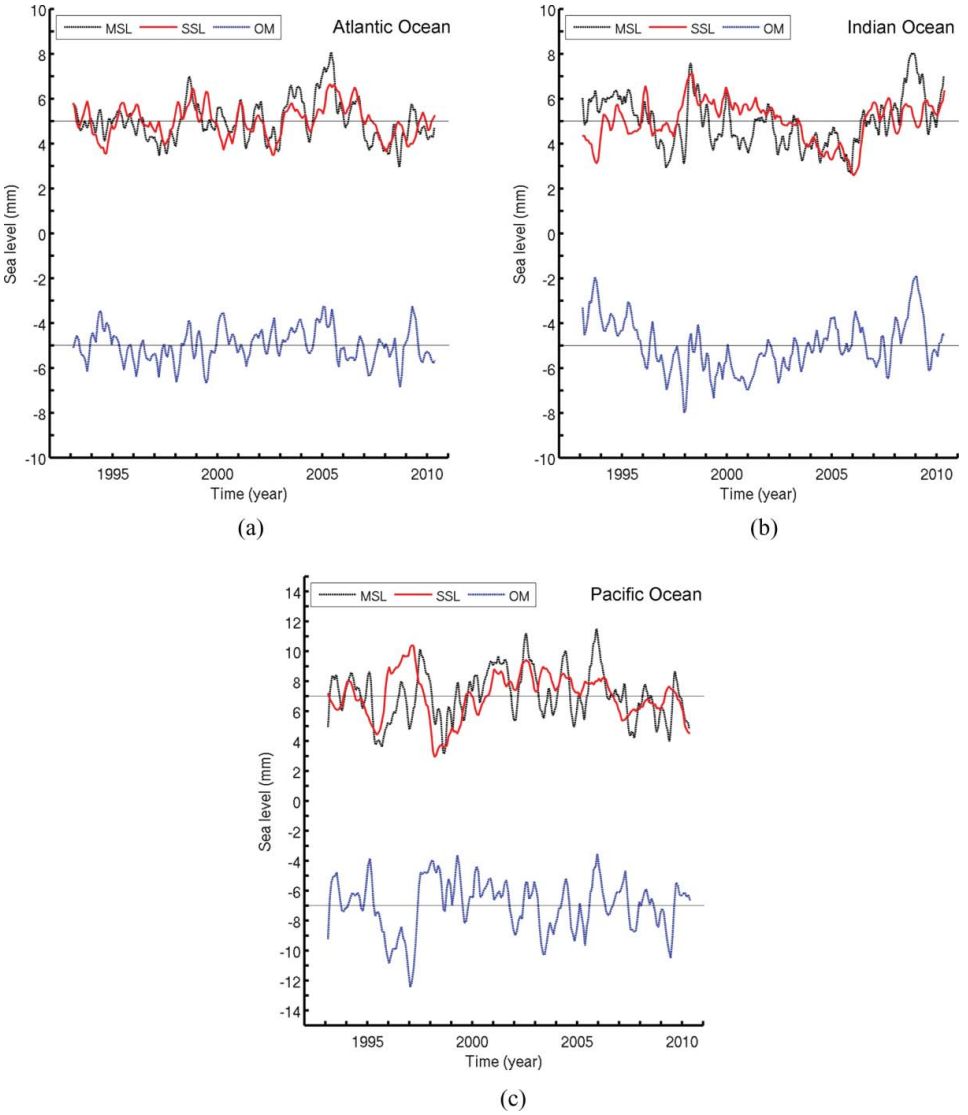

Figure 2. Contribution of the (a) Atlantic, (b) Indian, and (c) Pacific basins to the global mean sea level: area-averaged mean sea level (MSL, black curve), area-averaged mean steric sea level (SSL, red curve) and ocean mass component (difference between the former two) (OM, blue curve). See text for basin boundaries. Units are mm (sea level equivalent). The MSL/SSL and OM time series are shifted vertically for clarity. Note that the time series are area-weighted (i.e., multiplied by the ratio between the surface of considered region and the whole ocean surface). (Color figure available online.)

latitudinal band. To further detail the importance of such an anomaly, the top inset in Figure 3 represents the (reverse) total land water storage time series expressed in equivalent sea level (as in Figure 1b), and the right-hand side inset shows the correlations (computed over the 1993–2008 and 1996–2000 timespans; respectively, black and red curves) between the land water time series and the Pacific mass anomalies within successive 1° latitudinal bands. The right-hand side curves shows that positive correlations are obtained in the north tropical domain, with correlation maxima (reaching 0.8) around the equator, 10°N and 20°N. In the following, we consider the 0°–25°N latitudinal band for the tropical Pacific mass anomaly.

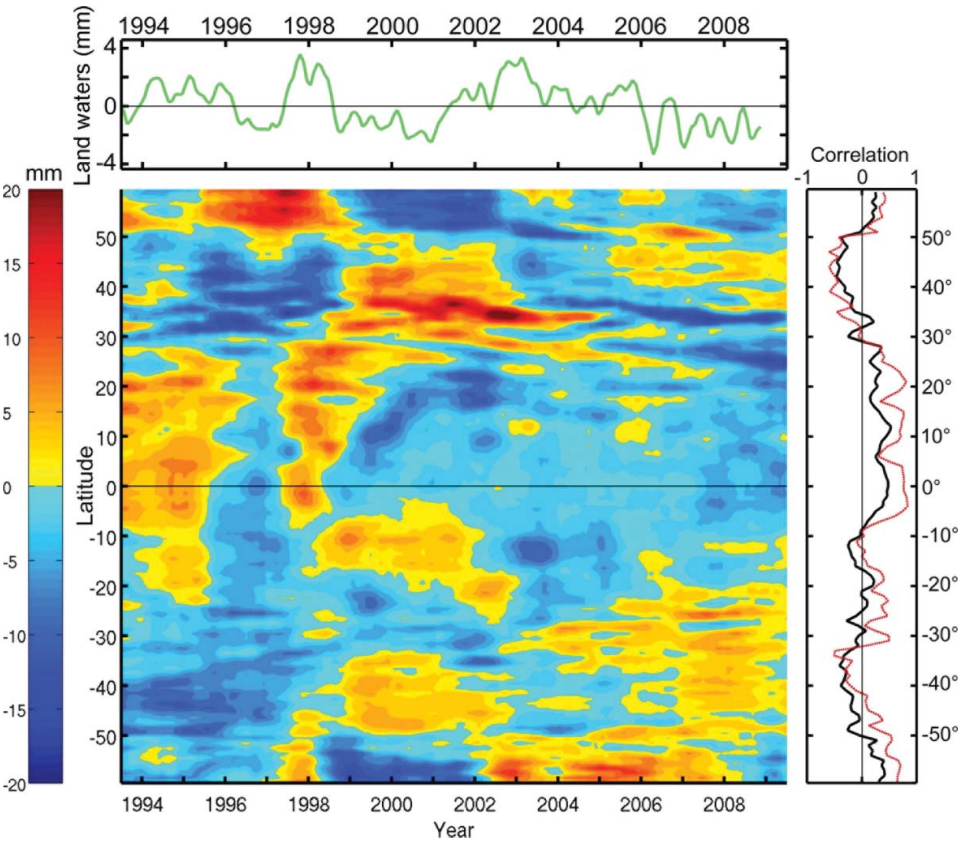

Figure 3. Time-latitude diagram of the zonally averaged (from 120°E to the American coasts) Pacific ocean mass component. Values have been smoothed with a 6-month running mean for clarity. Units: mm (sea level equivalent). The top curve represents the reversed total land water storage time series expressed in equivalent sea level, as in Figure 1b. The right-hand side black and red curves are the correlations as a function of latitude between the land water storage curve (in equivalent sea level) and Pacific ocean mass in successive 1° wide latitudinal bands over the whole timespan and over 1996–2000, respectively. (Color figure available online.)

But tests have shown that considering slightly different bands (e.g., 5°S–25°N or 0°–30°N) leads to essentially similar results. Note also that considering a longitude area as of 100°E instead of 120°E (i.e., including the South China Sea) does not change these results.

To determine the zonal extension of the 0°–25°N mass anomaly, we computed a longitude-time diagram of the mass anomalies shown in Figure 4. In Figure 4 we observe a band of positive mass anomalies during the 1997/1998 El Nino extending from about 120°E–140°E to the coast of America. In contrast, we note a band of negative anomalies located in the central tropical Pacific during the 1999/2000 La Nina.

To check whether the north tropical Pacific mass anomaly quantitatively correlates with (i.e., is compensated by) the total land water storage change, we restricted the analysis done for Figure 2c to the 0°–25°N tropical Pacific. The corresponding altimetry-based sea level, steric sea level, and ocean mass time series are shown in Figure 5 (with area-weighting). On the ocean mass curve we have superimposed the (reversed) total land water

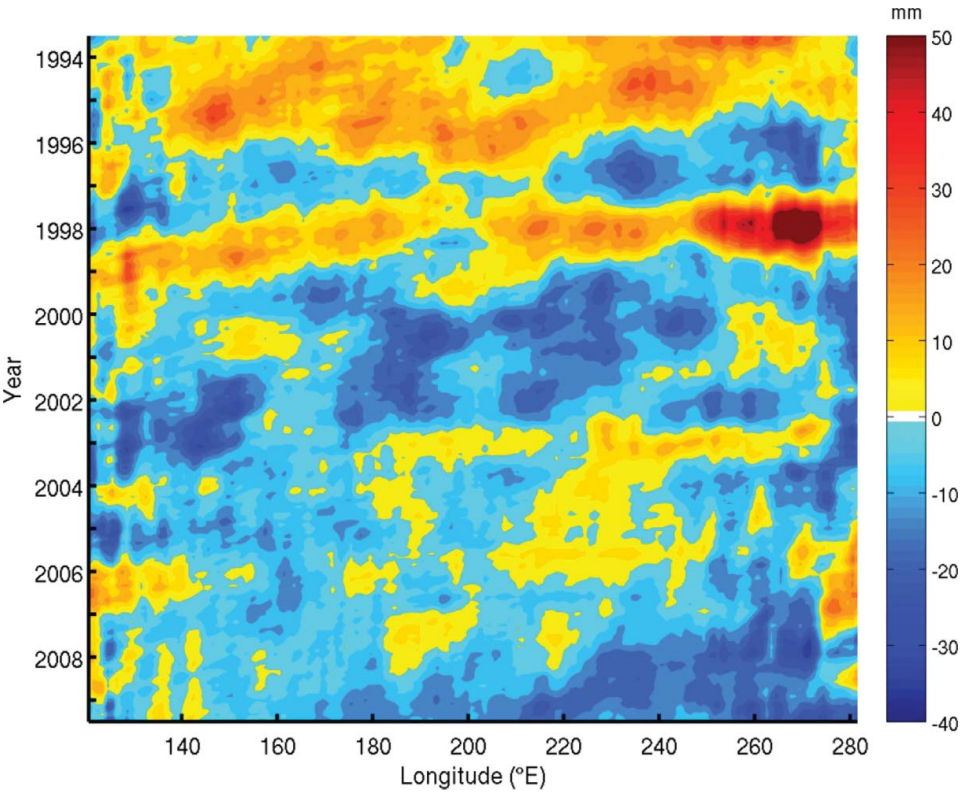

Figure 4. Longitude-time diagram of meridionally averaged Pacific ocean mass component (data averaged in latitude between 0° and 25°N). Values have been smoothed with a 6-month running mean for clarity. Units: mm (sea level equivalent). (Color figure available online.)

curve (expressed in equivalent sea level). We note an overall good agreement and a quasi perfect quantitative agreement during the 1997/1998 El Nino, indicating that total land water deficit during that El Nino was almost totally compensated by an increase of the north tropical Pacific Ocean mass. The correlation between north tropical Pacific Ocean (0°–25°N) mass and land water storage (expressed in equivalent sea level) amounts to 0.91 over 1997–98 (considering slightly different latitudinal bands for the ocean mass averaging, e.g., 0°–30°N, has negligible influence on the shape of the curve shown in Figure 5, as well as on the correlation).

4. Discussion

In Section 3, we showed that the 1997/1998 positive anomaly of the (detrended) GMSL is largely due to an excess of mass located in a zonal band of the north tropical Pacific Ocean between ∼0° and 25°N latitude. We also showed that this north tropical Pacific mass excess quantitatively compensates the total land water storage deficit observed during that El Nino event. The question now is: Which process causes the 1997/1998 El Nino-related north tropical Pacific positive mass anomaly?

A budget analysis of all terms involved in the mass conservation equation would be necessary to solve that question. While this is not possible with the observation data we

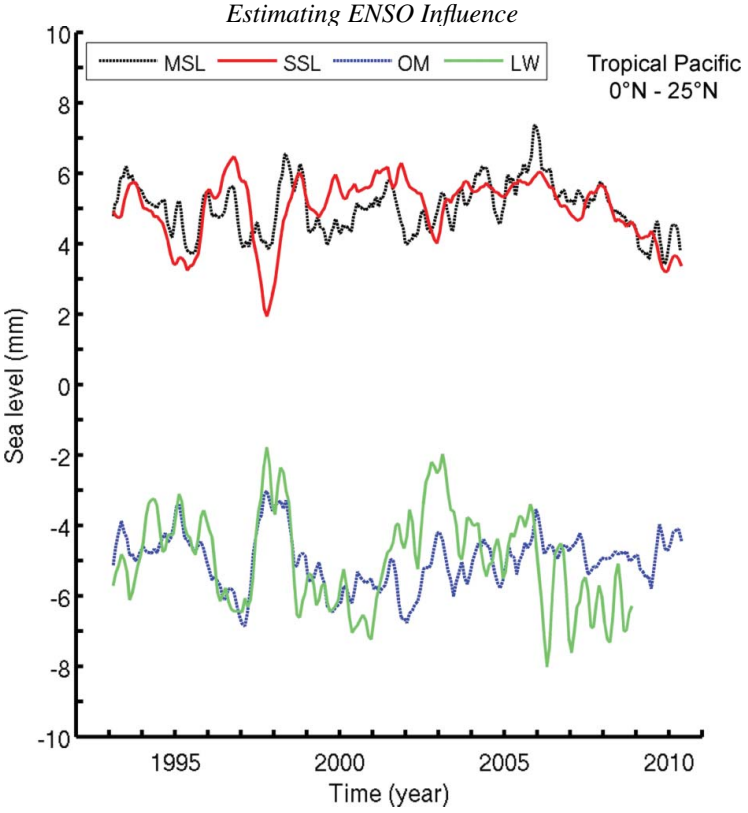

Figure 5. Contribution of the tropical north Pacific (0–25°N) to the GMSL: mean sea level, MSL (black curve), steric sea level, SSL (red curve) and ocean mass component (difference between the former two), OM (blue curve). The reversed total land water time series (expressed in equivalent sea level) LW (green curve) is superimposed. The MSL/SSL, OM/LW time series are shifted vertically for clarity. Units: mm (sea level equivalent). (Color figure available online.)

have in hand, we do believe instructive to present tentative explanations that may stimulate ocean modellers and/or new ideas. In the following, we examine successively different terms of the mass budget equation over the north tropical Pacific Ocean (0°–25°N).

Given our definition of the north tropical Pacific in terms of area (i.e., between 0° and 25°N latitude and ~120°E to the American coasts) its mass changes can be due to variations of surface P-E, river runoff (R), and water mass transports across the open boundaries. The mass balance equation can then be written as:

$$\mathrm{dOM/dt} = \mathrm{P} - \mathrm{E} + R + \mathrm{Inflow/Outflow} \tag{3}$$

In Eq. (3), dOM/dt is the time derivative of the north tropical Pacific ocean mass (area defined above). The term called Inflow/Outflow (denoted I/O in the following) represents transport of water in and out the considered domain (counted positive when entering the domain). The I/O term results from: (1) flow across the equator via the interior pathway and the western boundary current, (2) flow across the 25°N parallel, and (3) flow at the western boundary (i.e., the Indonesian throughflow-ITF; Gordon 2005). Note that R in Eq. (3) can be neglected as no major river flows into the considered region.

In the following two subsections, we estimate the two dominant terms of the right-hand side of the water budget equation (Eq. (3)), that is, net precipitation (P-E) (subsection 4.1)

and Inflow/Outflow (I/O; subsection 4.2). Corresponding analysis is performed over the 0–25°N tropical Pacific.

4.1. (P-E) Changes over the North Tropical Pacific Ocean (0–25°N)

ENSO events produce large scale anomalies of the atmospheric circulation in the tropics, with direct effects on precipitation (e.g., Dai and Wigley 2000; Trenberth et al. 2002; Neelin et al. 2003; Smith et al. 2006). Warm ENSO events (El Nino) give rise to more rainfall over the oceans and less rainfall over land, with opposite variations during cold events (La Nina) (Gu et al. 2007). Gu et al. (2007) and Gu and Adler (2011) showed that strong positive/negative precipitation anomalies affect tropical ocean/land during ENSO warm phases, with ocean/land responses being always opposite in sign. They also showed that the ENSO-related total precipitation signal in the tropics (ocean plus land) is weak. Dai and Wigley (2000) and Curtis and Adler (2003) showed how precipitation patterns evolve in the tropical Pacific during the ENSO development. For example, El Nino produces positive precipitation anomalies in the central equatorial Pacific that move eastward and southward as the event matures.

We computed P-E time series using the different meteorological datasets described in Section 2.4. Figure 6a shows the P-E time series over the 0–25°N tropical Pacific from the different datasets between 1993 and 2009. This graph clearly shows a high correlation between the different computations (mean standard deviation of 0.44 mm/month over the whole period) and particularly during the 1997/1998 El Nino event. Figure 6b compares the net precipitation mean (averaging all individual time series) and associated standard deviation (red curve and shading) with the dOM/dt time series (blue curve). Their difference is shown in Figure 6c. Figure 6b indicates a reasonably good correlation between mean net precipitation and dOM/dt (correlation of 0.58) during the whole timespan. However, during the 1997/1998 El Nino peak, dOM/dt is less negative than P-E. The difference curve (Figure 6c) indeed shows a large positive residual peaking in early 1998, indicating that there is no compensation between dOM/dt and P-E; thus, the I/O term appearing in Eq. (3) may not be neglected. The result shown in Figure 6c corroborates the fact that changes in net precipitation cannot to be directly responsible for the north tropical Pacific mass anomaly because of fast water spreading at the surface by the ocean currents (see Huang et al. 2005).

4.2. Mass Transport into and out from the North Tropical Pacific Ocean (0–25°N)

In the following, we examine the inflow/outflow term of the north tropical Pacific water budget.

Figure 7 shows the I/O term (difference between dOM/dt and P-E) over the north tropical Pacific (0–25°N) (same as Figure 6c but over 1996–2000 only to enhance the 1997/1998 ENSO period) on which is superimposed the negative I/O (i.e., -I/O) term computed as the difference between dOM/dt and P-E over the whole Indian Ocean and whole south Pacific domain (0–60°S). Looking at Figure 7, we clearly see a high anti-correlation (−0.95) between the inflow/outflow terms of these two regions. Figure 7 also shows the I/O term over the northern part of the Pacific Ocean (25°N–60°N) (green curve). The corresponding curve is rather flat, with very small interannual variations compared with the two other curves, indicating that water transfers in/out the 25°N parallel are almost balanced.

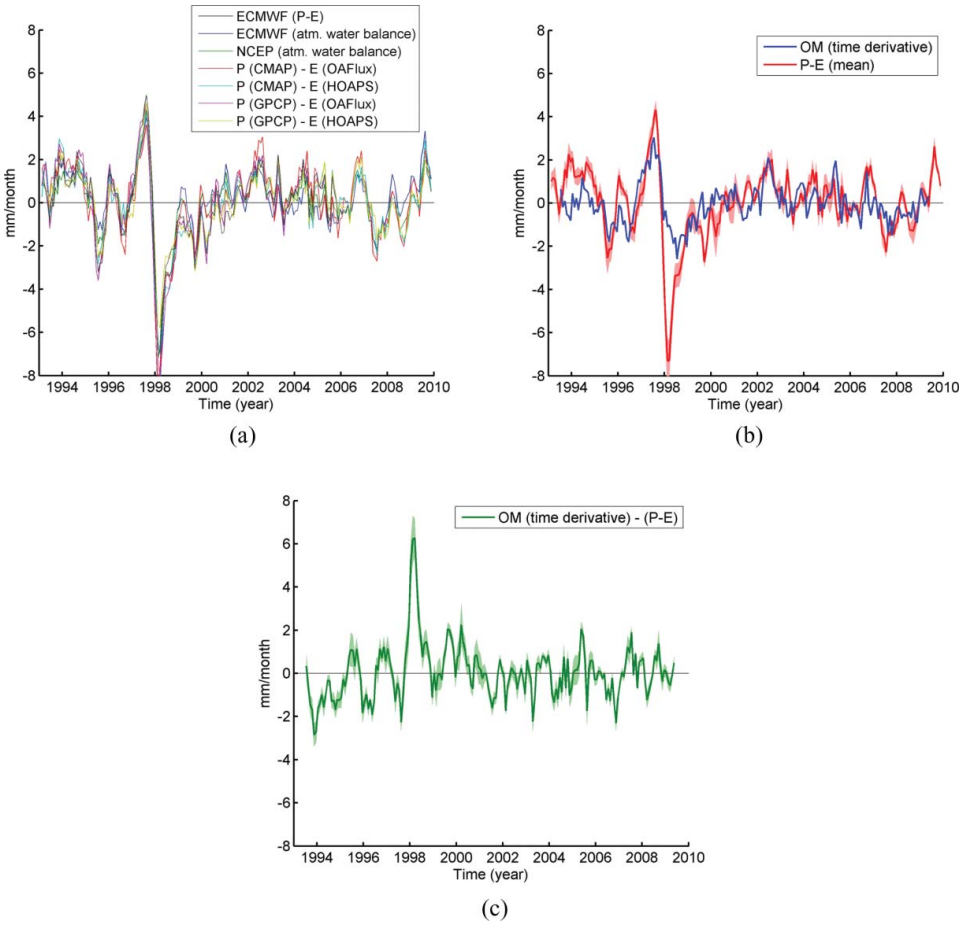

Figure 6. (a) Direct and indirect (from atmospheric water balance) estimates of net P-E over the north Pacific Ocean (0–25°N) from different meteorological data sets. (b) Time derivative of the mass component (blue curve) and mean P-E (red curve) values averaged over the North Pacific Ocean (0–25°N). (c) Difference time series between the time derivative of the North Pacific Ocean mass component and mean (P-E). Red and green shadings in Figures 6a and 6b represent spreading the P-E estimates. Unit: mm/month. (Color figure available online.)

The reported anti-correlation between the inflow/outflow terms of the north tropical Pacific (0–25°N) and the combined Indian oceans plus south Pacific domain suggests that the water exchanges with the Atlantic Ocean at the eastern and western boundaries are also compensated.

The above two results suggests that the positive mass anomaly in the north tropical Pacific is linked to flow variations across the equator via the interior pathway and the western boundary current and/or variations of the Indonesian throughflow (ITF). We briefly discuss the latter possibility.

The Makassar Strait located between Borneo and Sulawesi is the main channel for the ITF, carrying about 80% of the total ITF, which amounts to 15 Sv (Sv = 10^6 m^3/s) (Gordon et al. 2010). On average, the depth-integrated transport at the Makassar Strait is on the order of 8–12 Sv (Gordon 2005; Gordon et al. 2008), but interannual variability of

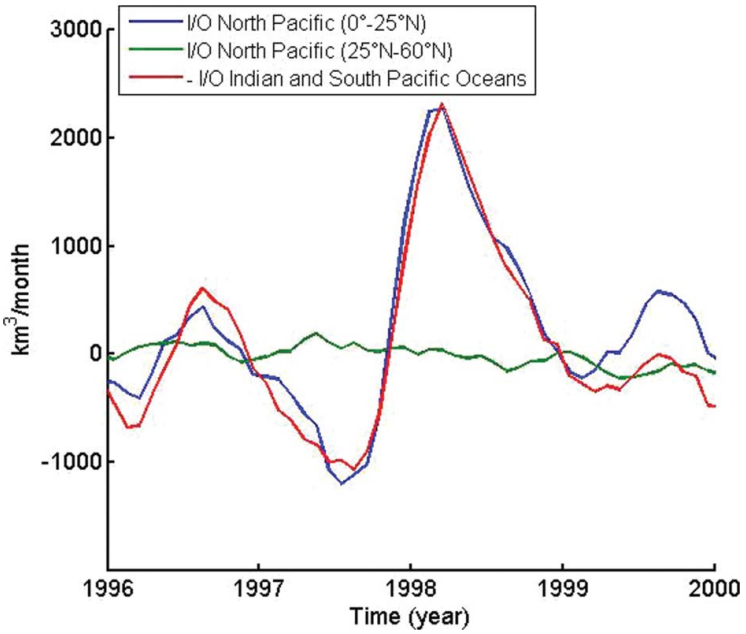

Figure 7. Time series of the difference (term I/O in Eq. (3)) between the time derivative of the ocean mass component and (P-E) for (blue curve) the north tropical Pacific Ocean (0–25°N) and (red curve) the Indian ocean plus south Pacific domain. Note that the sign of the red curve has been reversed to ease the comparison. The green curve represents the I/O term across the 25°N parallel in the north Pacific. Units are in km^3/month (i.e., data are multiplied by the areas of the considered domains). (Color figure available online.)

the ITF associated with ENSO has been reported (e.g., England and Huang 2005; Vranes and Gordon 2005). From in situ measurements, Susanto and Gordon (2005) showed that during the calendar year 1997, the Makassar transport was 7.9 Sv, falling to less than 5 Sv during the peak of the 1997/1998 El Nino. During 2004–06, the ENSO phase was generally that of El Niño (with a brief La Niña phase in early 2006), though substantially subdued relative to the 1997/1998 event. The 2004–06 Makassar Strait transport averaged 11.6 Sv (Gordon et al. 2008; Gordon et al. 2010). During 2007–10, when the ENSO phase shifted toward La Niña, a single current measuring mooring in Makassar Strait observed elevated southward velocity, with an estimated transport of 13–14 Sv (Gordon et al. 2012). Surface water from the tropical Pacific is lost as the Mindanao Current leaks into the ITF; that is, not all of the Mindanao Current turns eastward to feed into the Pacific's North Equatorial Counter Current. In this way, the ITF does act to redistribute the mass input from rainfall. Gordon et al. (2012) showed that the leakage of surface water from the Mindanao Current into the ITF is reduced during El Niño when the surface layer is drawn more from the 19°N Luzon Strait throughflow to enter Makassar Strait from the South China Sea. During La Nina, the Luzon Strait throughflow goes to near zero allowing greater surface layer inflow from the Mindanao. Such water transport changes are related to large-scale wind field changes over the Pacific and Indian oceans during ENSO (e.g., Godfrey 1996).

Reduced ITF of a few Sv, if not compensated by flow variations across the equator, is of the right order of magnitude to explain the north tropical Pacific mass excess observed during the 1997/1998 El Nino peak. In effect, a crude calculation shows that

1 Sv reduction over 1 month corresponds to a water volume of 2600 km^3 remaining in the north tropical Pacific while the observed mass excess in this region corresponds to $\sim$1500 km^3.

The above results may suggest that the 1997/1998 El Nino event could be related to an important variation of the water mass transfer between the north tropical Pacific Ocean (0–25°N) and Indian and South Pacific oceans. In particular, a reduction of the ITF possibly combined with an intensification of water transfers from the south Pacific could have led to an important water mass increase in the north tropical Pacific region. Even though this study does not allow us to discriminate between the relative importance of these contributions, we cannot exclude that an important part of the water transport variations may have occurred at the Makassar Strait. Further quantitative analyses are required to confirm this, for example, using ocean general circulation model outputs.

5. Conclusion

The results presented in this study confirm that interannual variability of the GMSL has essentially a water mass origin, as the interannual GMSL is highly inversely correlated with total land water storage change, in particular during ENSO events. Focusing on the large positive GMSL anomaly observed during the 1997/1998 El Nino, we show that this anomaly is largely due to a mass excess of the north tropical Pacific (located between 0° and 25°N in latitude and $\sim$120°E to the American coasts in longitude). We also show that the ocean-atmosphere water budget computed over the north tropical Pacific (0–25°N) is not closed during the 1997/1998 El Nino peak if the inflow/outflow terms are not accounted for. The north tropical Pacific mass excess associated with this El Nino event is consistent with the reduced depth-integrated water transport at the Makassar Strait (the Indonesian throughflow) previously reported during the 1997/1998 El Nino, although we cannot exclude that flow across the equator via the interior pathway and the western boundary current also play some role. Further analyses are required to quantitatively confirm or infirm this conclusion.

A similar investigation should be performed for La Nina events, during which important drops of the GMSL are observed. This was the case, for example, in 2007–08 and 2010–11. It will be interesting to determine whether the transport at the Makassar Strait is also a good candidate to explain the GMSL variability, as well as to assess the potential role of meridional mass transports across the equator. In line with our observation-based results, a precise quantification of all processes responsible for the GMSL at the ENSO time scale will be conducted with the help of ocean general circulation model outputs.

Acknowledgements

O. Henry, S. Munier, W. Llovel, and H. Palanisamy are supported, respectively, by a European grant in the context of the Monarch Project, a postdoctoral grant from CNES, a postdoctoral grant from JPL/NASA, and the French ANR CECILE project. A. L. Gordon research is supported by the National Science Foundation grant OCE-0725935. This is Lamont-Doherty contribution number 7545.

We thank H. Douville, B. Decharme, and R. Alkama for providing us with the ISBA-TRIP model outputs.

References

Ablain, M., A. Cazenave, S. Guinehut, and G. Valladeau. 2009. A new assessment of global mean sea level from altimeters highlights a reduction of global slope from 2005 to 2008 in agreement with in-situ measurements. *Ocean Sci.* 5(2):193–201.

Adler, R. F., G. J. Huffman, A. Chang, R. Ferraro, P. P. Xie, J. Janowiak, B. Rudolf, U. Schneider, S. Curtis, D. Bolvin, A. Gruber, J. Susskind, P. Arkin, and E. Nelkin. 2003. The version-2 global precipitation climatology project (GPCP) monthly precipitation analysis (1979–present). *Journal of Hydrometeorology* 4:1147–1167.

Alkama, R., B. Decharme, H. Douville, A. Voldoire, S. Tyteca, P. Le Moigne, M. Becker, A. Cazenave, and J. Sheffield. 2010. Global evaluation of the ISBA-TRIP continental hydrological system Part 1: Comparison to GRACE terrestrial water storage estimates and in-situ river discharges. *Journal of Hydrometeorology* 11:583–600. doi: 10.1175/2010JHM1211

Andersson, A., S. Bakan, K. Fennig, H. Grassl, C. Klepp, and J. Schulz. 2007. Hamburg ocean atmosphere parameters and fluxes from satellite data – HOAPS-3 – monthly mean. *World Data Center for Climate electronic publication*.

Bindoff, N., J. Willebrand, V. Artale, A. Cazenave, J. Gregory, S. Gulev, K. Hanawa, C. Le Quéré, S. Levitus, Y. Nojiri, C. K. Shum, L. Talley, and A. Unnikrishnan. 2007. Observations: Oceanic climate and sea level. In ed. S. Solomon, D. Qin, M. Manning, Z. Chen, M. Marquis, K. B. Averyt, M. Tignor, and H. L. Miller, *Climate Change 2007: The Physical Science Basis. Contribution of Working Group I to the Fourth Assessment Report of the Intergouvernmental Panel on Climate Change*. Cambridge: Cambridge University Press.

Cazenave, A., and W. Llovel. 2010. Contemporary sea level rise. *Annual Review in Marine Science* 2:145–173.

Church, J. A., N. J. White, L. F. Konikow, C. M. Domingues, J. G. Cogley, E. Rignot, J. M. Gregory, M. R. van den Broeke, A. J. Monaghan, and I. Velicogna. 2011. Revisiting the Earth's sea level and energy budgets from 1961 to 2008. *Geophys. Res. Lett.* 38:L18601. doi: 10.1029/2011GL048794

Curtis, S., and R. F. Adler. 2003. Evolution of El Nino-precipitation relationships from satellites and gauges. *J. Geophys. Res.* 108:4153. doi: 10.1029/2002JD002690

Dai, A., and T. M. L. Wigley. 2000. Global patterns of ENSO-induced precipitation. *Geophys. Res. Lett.* 27(9):1283–1286.

Decharme, B., and H. Douville. 2006. Introduction of a sub-grid hydrology in the ISBA land surface model. *Climate Dyn.* 26:65–78.

England, M., and F. Huang. 2005. On the interannual variability of the Indonesian throughflow and its linkage with ENSO. *J. Clim.* 18:1435–1444.

Godfrey, J. S. 1996. The effect of the Indonesian throughflow on ocean circulation and heat exchange with the atmosphere: A review. *J. Geophys. Res.* 101(C5):12217–12237.

Gordon, A. L. 2005. Oceanography of the Indonesian seas and their throughflow. *Oceanography* 18(4):14–27.

Gordon, A. L., R. D. Susanto, A. Ffield, B. A. Huber, W. Pranowo, and S. Wirasantosa. 2008. Makassar Strait throughflow, 2004 to 2006. *Geophys. Res. Letters* 35:L24605. doi: 10.1029/2008GL036372

Gordon, A. L., J. Sprintall, H. M. Van Aken, D. Susanto, S. Wijffels, R. Molcard, A. Ffield, W. Pranowo, and S. Wirasantosa. 2010. The Indonesian throughflow during 2004–2006 as observed by the INSTANT program. Modeling and observing the Indonesian throughflow. In Ed. A. L. Gordon and V. M. Kamenkovich, *Dynamics of Atmosphere and Oceans* 50:115–128.

Gordon, A. L., B. A. Huber, E. J. Metzger, R. D. Susanto, H. E. Hurlburt, and T. R. Adi. 2012. South China Sea throughflow impact on the Indonesian throughflow. *Geophys. Res. Lett.* (in revision).

Gu, G., R. F. Adler, G. J. Huffman, and S. Curtis. 2007. Tropical rainfall variability on interannual to interdecadal and longer time scales derived from the GPCP monthly products. *J. Climate* 20:4033–4046.

Gu, G., and R. F. Adler. 2011. Precipitation and temperature variations on the interannual time scale: Assessing the impact of ENSO and volcanic eruptions. *J. Climate* 24:2258–2270.

Huang, B. Y., V. M. Mehta, and N. Schneider. 2005. Oceanic response to idealized net atmospheric freshwater in the Pacific at the decadal time scale. *J. Phys. Oceanography* 35(12):2467–2486. doi: 10.1175/JPO2820.1

Ishii, M., and M. Kimoto. 2009. Reevaluation of historical ocean heat content variations with varying XBT and MBT depth bias corrections. *Journal of Oceanography* 65:287–299.

Kalnay, E., M. Kanamitsu, R. Kistler, W. Collins, D. Deaven, L. Gandin, M. Iredell, S. Saha, G. White, J. Woollen, Y. Zhu, M. Chelliah, W. Ebisuzaki, W. Higgins, J. Janowiak, K. C. Mo, C. Ropelewski, J. Wang, A. Leetmaa, R. Reynolds, R. Jenne, and D. Joseph. 1996. The NCEP/NCAR 40-year reanalysis project. *Bulletin of the American Meteorological Society* 77:437–471.

Levitus, S., J. I. Antonov, T. P. Boyer, R. A. Locarnini, H. E. Garcia, and A. V. Mishonov. 2009. Global ocean heat content 1955–2008 in light of recently revealed instrumentation problems. *Geophys. Res. Lett.* 36:L07608. doi: 10.1029/2008GL037155

Llovel, W., M. Becker, A. Cazenave, S. Jevrejeva, R. Alkama, B. Decharme, H. Douville, M. Ablain, and B. Beckley. 2011a. Terrestrial waters and sea level variations on interannual time scale. *Global Planet Change* 75:76–82. doi: 10.1016/j.gloplacha.2010.10.008

Llovel, W., B. Meyssignac, and A. Cazenave. 2011b. Steric sea level variations over 2004–2010 as a function of region and depth: Inference on the mass component variability of the North Atlantic. *Geophys. Res. Lett.* 38:L15608. doi: 101029/2011GL047411

Neelin, J. D., C. Chou, and H. Su. 2003. Tropical drought regions in global warming and El Nino teleconnections. *Geophys. Res. Lett.* 30:2275. doi: 10.1029/2003GL018625

Nerem, R. S., D. P. Chambers, C. Choe, and G. T. Mitchum. 2010. Estimating mean sea level change from the TOPEX and Jason altimeter missions. *Marine Geodesy* 33(1):435–446.

Oki, T., and Y. C. Sud. 1998. Design of total runoff integrating pathways (TRIP)—a global river channel network. *Earth Interactions* 2(1):1–37.

Sahoo, A. K., M. Pan, T. J. Troy, R. K. Vinukollu, J. Sheffield, and E. F. Wood. in press. Reconciling the global terrestrial water budget using satellite remote sensing. *Remote Sensing of Environment*.

Simmons, A., S. Uppala, D. Dee, and S. Kobayashi. 2007. Era-interim: New ECMWF reanalysis products from 1989 onwards. *ECMWF Newsletter* 110.

Smith, T. M., X. Yin, and A. Gruber. 2006. Variations in annual global precipitation (1979–2004), based on the global precipitation climatology project 2.5° analysis. *Geophys. Res. Lett.* 33:L06705. doi: 10.1029/2005GL025393

Susanto, R. D., and A. L. Gordon. 2005. Velocity and transport of the Makassar Strait throughflow. *J. Geophys. Res.* 110:C01005. doi: 10.1029/2004JC002425

Syed, T. H., J. S. Famiglietti, and D. P. Chambers. 2009. GRACE-based estimates of terrestrial freshwater discharge from basin to continental scales. *Journal of Hydrometeorology* 10:22–40.

Trenberth, K. E., J. M. Caron, D. P. Stepaniak, and S. Worley. 2002. Evolution of El Nino-southern oscillation and global atmospheric surface temperatures. *J. Geophys. Res.* 107:4065. doi: 10.1029/2000JD000298

Vranes, K., and A. L. Gordon. 2005. Comparison if Indonesian troughflow transport observations, Makassar Strait to eastern Indian Ocean. *Geophys. Res. Lett.* 32:L10606. doi: 10.1029/2004GL022158

Wolter, K., and M. S. Timlin. 1998. Measuring the strength of ENSO—how does 1997/98 rank? *Weather* 53:315–324.

Xie, P. P., and P. A. Arkin. 1997. Global precipitation: A 17-year monthly analysis based on gauge observations, satellite estimates, and numerical model outputs. *Bulletin of the American Meteorological Society* 78:2539–2558.

Yu, L., and R. A. Weller. 2007. Objectively analyzed air-sea heat fluxes for the global ice-free oceans (1981–2005). *Bull. Amer. Meteorol. Soc.* 88(4):527–539.